Faraday Rotation Due to Excitation of Magnetoplasmons in Graphene Microribbons

Mykhailo Tymchenko,[†,⊥] Alexey Yu. Nikitin,[‡,§] and Luis Martín-Moreno[†,*]

[†]Instituto de Ciencia de Materiales de Aragón and Departamento de Física de la Materia Condensada, CSIC-Universidad de Zaragoza, 50009 Zaragoza, Spain, [‡]CIC nanoGUNE Consolider, 20018 Donostia-San Sebastián, Spain, and [§]Ikerbasque, Basque Foundation for Science, 48011 Bilbao, Spain. [⊥]Present address: Department of Electrical and Computer Engineering, The University of Texas at Austin, Austin, Texas 78712, USA.

ABSTRACT A single graphene sheet, when subjected to a perpendicular static magnetic field, provides a Faraday rotation that, per atomic layer, greatly surpasses that of any other known material. In continuous graphene, Faraday rotation originates from the cyclotron resonance of massless carriers, which allows dynamical tuning through either external electrostatic or magneto-static setting. Furthermore, the rotation direction can be controlled by changing the sign of the carriers in graphene, which can be done by means of an external electric field. However, despite these tuning possibilities, the requirement of large magnetic fields hinders the application of the Faraday effect in real devices, especially for frequencies higher than a few terahertz. In this work we demonstrate that large Faraday rotation can be achieved in arrays of graphene microribbons, through the excitation of the magnetoplasmons of *individual* ribbons, at larger frequencies than those dictated by the cyclotron resonance. In this way, for a given magnetic field and chemical potential, structuring graphene periodically can produce large Faraday rotation at larger frequencies than what would occur in a continuous graphene sheet. Alternatively, at a given frequency, graphene ribbons produce large Faraday rotation at much smaller magnetic fields than in continuous graphene.

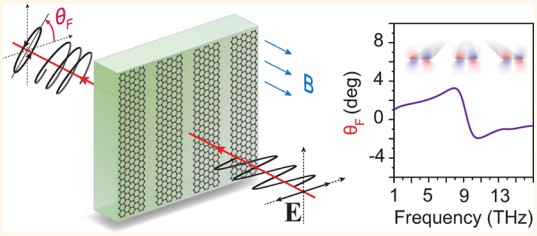

KEYWORDS: graphene ribbons · magnetic field · Faraday rotation · graphene magnetoplasmons (GMP)

The polarization of a plane wave is rotated when light passes through a transparent media in the presence of a perpendicular static magnetic field B. This phenomenon, known as Faraday rotation, has important applications in optical diodes,[1] sensing and magnetic microscopy,[2] *etc.* Usually, Faraday rotation requires the presence of ferromagnets, as typical Faraday rotation angles (θ_F) are small in nonmagnetic media (smaller than 0.01°/T even) for plasmon-assisted metallic structures in the optical regime[3]).

Recently, a single graphene sheet has been found to show extremely large Faraday angles. At frequencies smaller than ~0.1 THz, θ_F is virtually frequency-independent and can be of the order of tens of degrees for $B \sim 1$ T.[4] At larger frequencies (~1 THz), a continuous graphene sheet presents very large Faraday rotation ($\theta_F \approx 6°$ at $B = 7$ T) originating from the excitation of the cyclotron resonance.[5]

These remarkable findings have prompted the search for mechanisms capable of extending the range at which graphene structures present substantial θ_F to larger frequencies and/or smaller magnetic fields. One possibility is to introduce small periodic gaps in the graphene sheet, thus creating a metasurface with an enhanced effective capacitance and, correspondingly, a blue-shifting in the Faraday rotation maximum (θ_F of the order of a few degrees at ~5 THz for $B = 7$ T).[6] A different mechanism is to involve the resonant excitation of magnetoplasmon modes in the graphene sheet. This mechanism has been invoked to explain the Faraday rotation experimentally detected in graphene grown on SiC, where plasmons can be excited due to the breaking of translational symmetry induced by substrate defects.[7] In that work, however, coherent excitation of plasmons is hampered by the existing distribution of sizes and shapes of the homogeneous graphene regions.

In this paper, we will explore the possibility of using disconnected geometries supporting graphene surface plasmons, that

* Address correspondence to lmm@unizar.es.

Received for review June 27, 2013 and accepted September 30, 2013.

Published online September 30, 2013
10.1021/nn403282x

can be resonantly excited by incident radiation, in order to enhance the Faraday rotation. In common with the metasurfaces involving physical gaps in graphene, we will considered periodic arrays, but our proposal relies on the plasmonic resonances of the *individual* (disconnected) basic structures composing the periodic system.

At zero magnetic field, coupling to graphene plasmons strongly enhances the interaction between graphene and incident radiation.[8−15] In the presence of a static magnetic field, applied perpendicularly to graphene, plasmons and cyclotron excitations hybridize, leading to the formation of graphene magnetoplasmons (GMP).[16−20] These GMP modes are known to significantly modify the magneto-optical response of graphene structures.[21−24]

Specifically, here we show that graphene ribbons can be used both to enlarge the frequency range and to reduce the magnetic field at which graphene structures present large Faraday rotation. Graphene plasmonic gratings, which combine giant Faraday rotation in graphene with strong coupling between radiation and graphene plasmons, provide the exciting prospect of dynamically tunable ultrathin devices in both THz and infrared regimes, by employing solely the magneto-optical properties of graphene. Additionally, the mechanism of excitation of resonances of individual ribbons could be further enhanced through the combination with other mechanisms, for instance by designing the capacitive inter-ribbon coupling (in the vein of the metasurface proposed in[6]), or through the combination with other materials (as the dielectric thin films used in plasmonic metal gratings to enhance the interaction time between light and plasmons[25]).

RESULTS AND DISCUSSION

In this paper, for proof of principle, we consider a periodic array of graphene ribbons (with width w and period L), illuminated at normal incidence by a monochromatic plane wave. A static magnetic field B is applied perpendicularly to the ribbons (see Figure 1 for a scheme of the considered geometry). The incident electric field is chosen to lie perpendicularly to the axis of the ribbon (p-polarization). In this way, any deviation in the direction of the transmitted electric field is due to the effect in the magnetic field, and not to a "filtering" effect arising from the different transmittances for s- and p-polarized waves, which would occur even at zero field.[26]

Graphene is represented by its semiclassical conductivity tensor:[27]

$$\sigma_{xx} = \sigma_{yy} = \frac{e^2|\mu_c|}{\hbar^2\pi}\frac{i(\omega+i/\tau)}{(\omega+i/\tau)^2-\omega_c^2}$$
$$\sigma_{xy} = -\sigma_{yx} = \frac{e^2|\mu_c|}{\hbar^2\pi}\frac{\omega_c}{(\omega+i/\tau)^2-\omega_c^2} \quad (1)$$

where μ_c is a chemical potential, τ is a relaxation time, and $\omega_c = eBv_F^2/|\mu_c|$ is the cyclotron frequency. Here v_F is the Fermi velocity of the Dirac fermions in graphene ($v_F = 9.5 \times 10^5$ m/s). We take a representative value for the chemical potential $\mu_c = 0.2$ eV. Our main conclusions are independent of this choice, but it must be noticed that the semiclassical expression for the conductivity incorporates only intraband transitions, *i.e.*, it is thus valid for frequencies $\hbar\omega < 2|\mu_c|$.[27−29] The spectral range we study in this paper is consistent with this restriction. We will consider two values for the relaxation time $\tau = 0.1$ ps (corresponding to the mobility of about 4500 $cm^2\ V^{-1}\ s^{-1}$), which is typical for experimentally studied graphene ribbons, and $\tau \simeq 4.4$ ps (corresponding to the mobility of 200 000 $cm^2\ V^{-1}\ s^{-1}$), which is expected to be achievable for suspended graphene if intrinsic disorder is eliminated.[30−32]

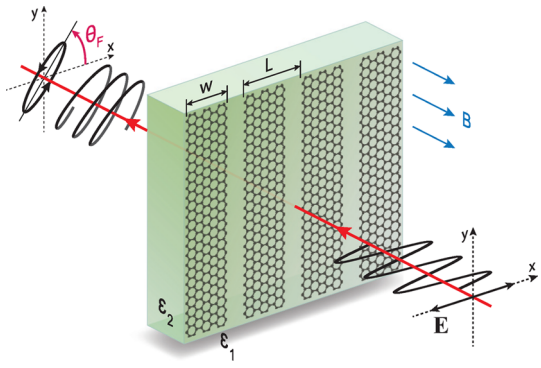

Figure 1. Schematic representation of the studied system: a plane monochromatic wave is normally incident onto the array of graphene ribbons, in the presence of a static perpendicular magnetic field B. θ_F is the Faraday rotation angle.

To find the scattering coefficients, we expand the total electromagnetic field in the conventional form of the Fourier-Floquet plane waves expansion, in both upper and lower semispaces. Matching appropriately the fields at the ribbon array yields an infinite set of equations for the amplitudes of these waves. Details of the method can be found in the Supporting Information. The numerical calculation of the amplitudes from the truncated system converges slowly (and what is worse, nonuniformly) with the number of diffraction orders considered. We have validated that results obtained by this method have converged by comparing them with those obtained by finite element calculations,[33] (which are more time-consuming), performed regularly for representative sets of parameters. When only the zero-order diffraction mode is radiative (*i.e*, when $L < \lambda$, which is the situation analyzed in this paper), the Faraday rotation angle can be computed from the amplitudes of the s and p transmitted plane waves, t_{0xx} and t_{0xy}, respectively, as:[34]

$$\theta_F = \frac{1}{2}\arg\frac{t_{0xx}-it_{0xy}}{t_{0xx}+it_{0xy}} \quad (2)$$

For zero magnetic field, the dependence of transmission, reflection, and absorption spectra of such

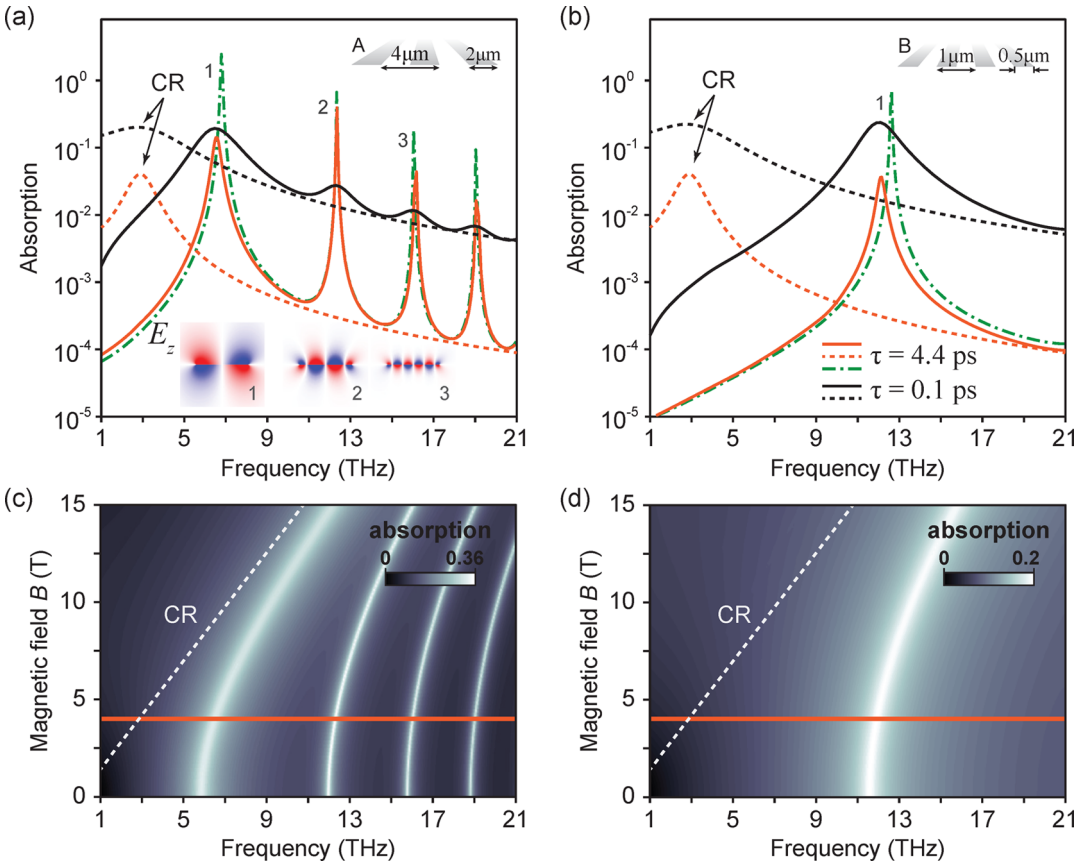

Figure 2. (a and b) Absorption spectra of two different ribbon arrays (continuous lines), with geometrical parameters specified in each panel, and a uniform graphene sheet (dashed curves), in a magnetic field $B = 4$ T. Two different relaxation times have been considered: $\tau = 4.4$ ps (orange curves) and $\tau = 0.1$ ps (black curves). Green dot-dashed curves show the absorption cross section for a single ribbon, for $\tau = 0.1$ ps. The structure of E_z at the first three resonances indicated with "1", "2", "3" is shown in the inset of (a). (c and d) The absorption of the arrays A and B (geometrical parameters specified in panels (a) and (b), respectively) as a function of both frequency and magnetic field B. White dashed lines indicate the position of the cyclotron resonance (CR) in a uniform graphene sheet. Orange solid lines indicate the position of the "cross sections" of this contour plot shown in panels a and b.

structures on both period and width of the ribbons has been extensively studied theoretically and experimentally.[8,11,13,35,36] In particular, it was found that the main resonance in the scattering coefficients is associated with the excitation of a hybridized mode, which is a linear combination of the two edge modes of the ribbon.[11,37,38] Additionally, there also exists an infinite set of weaker resonances which emerge due to coupling to waveguide-like graphene plasmons. As we will discuss below, in a perpendicular magnetic field the ribbon plasmon modes transform into magnetoplasmon excitations, but the number of modes and their field structure remains the same.

In what follows we study the magnetoresponse of two structures, representative of those used in recent experiments (performed at $B = 0$):[8] array "A", defined by ribbon width $w = 2\ \mu$m and period $L = 4\ \mu$m and array "B", with $w = 0.5\ \mu$m and $L = 1\ \mu$m.

Let us first analyze the absorption of radiation by the free-standing ribbon arrays ($\varepsilon_1 = \varepsilon_2 = 1$). In Figure 2a,b, we show the absorption for a continuous graphene sheet and for the arrays considered for the case $B = 4$ T. This figure also renders the absorption cross section of the corresponding single free-standing graphene ribbons showing that, for the geometrical parameters considered, the absorption resonances are essentially due to the GMPs of the individual ribbons; the inter-ribbon coupling results only in a slight red-shifting of the main absorption line. In the considered frequency range, where the conductivity is given by a Drude term, the ribbon GMP modes are similar to those studied in stripes of two-dimensional electron gases arising in GaAs heterostructures.[17,37−44] Those studies showed that the frequencies of the magnetoplasmon modes $\omega_n(B)$ are given by a simple expression

$$\omega_n(B) = \sqrt{\omega_n^2 + \omega_c^2} \qquad (3)$$

where ω_n is the set of plasmon frequencies in an isolated ribbon at zero magnetic field. Each eigenfrequency ω_n scales with the ribbon width as $(n/w)^{1/2}$, where n is a number of the mode, $n = 1, 2, 3, ...$[8,38] (only the odd orders are excited under the normal incidence). The dependence of the absorption spectra with DC

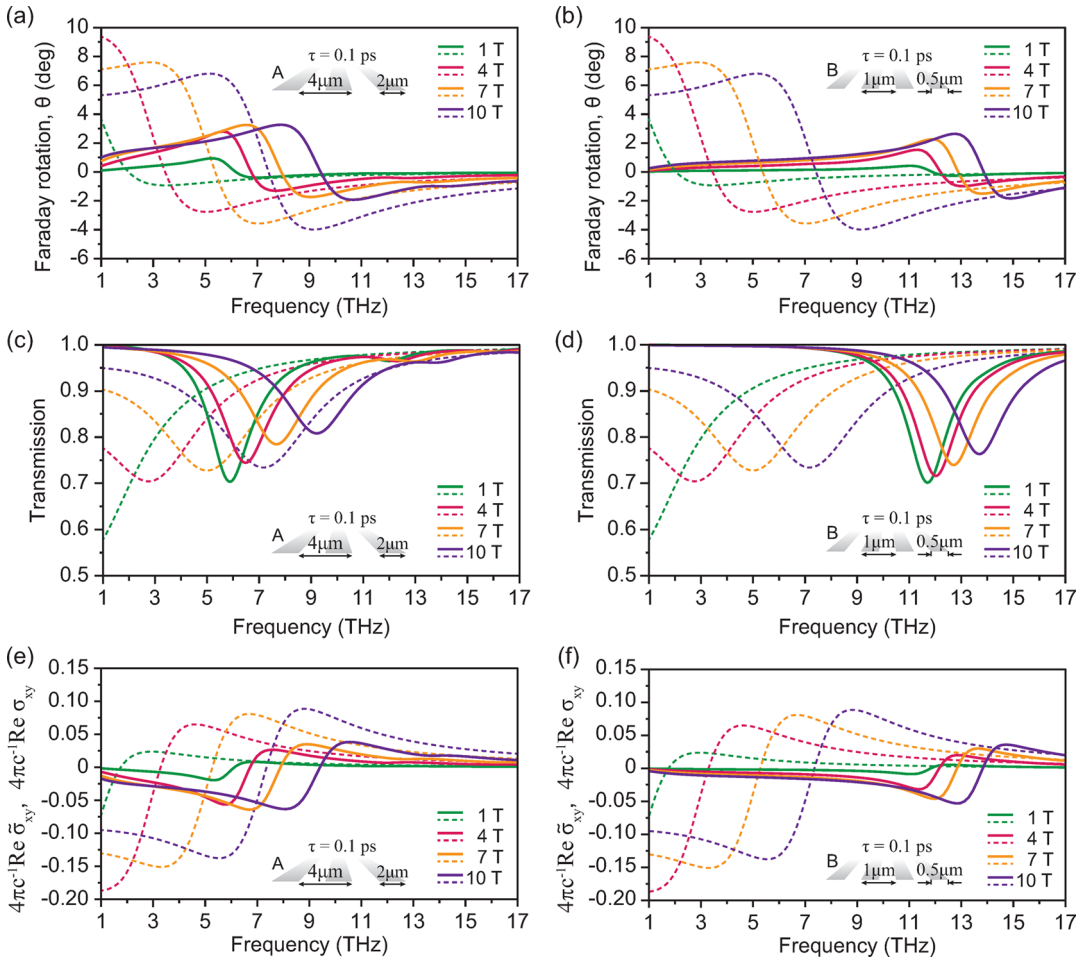

Figure 3. The results for ribbon arrays (solid curves) and continuous graphene (dashed curves) for relaxation time $\tau = 0.1$ ps. Panels to the left correspond to array "A" ($w = 2\ \mu$m, $L = 4\ \mu$m) while right panels are for array "B" ($w = 0.5\ \mu$m, $L = 1\ \mu$m). Upper panels: Faraday rotation angle at various magnetic fields. Middle panels: Zeroth-order transmission $|t_0|^2 = |t_{0xx}|^2 + |t_{0xy}|^2$. Lower panels: The real part of the nondiagonal component of the effective conductivity, $Re\tilde{\sigma}_{xy}$ (solid curves), and $Re\sigma_{xy}$ (dashed curves).

magnetic field for both arrays is rendered in Figure 2c,d, reflecting clearly the evolution of the GMP frequencies.

Figure 3a,b shows the spectra for the Faraday rotation angle for the two ribbon arrays considered, and for different DC magnetic fields (solid lines). For comparison, in the same panels we present the Faraday rotation angle for a continuous graphene sheet (dashed lines). As mentioned above, in continuous graphene the main resonance feature is associated to the cyclotron resonance. Therefore, giant Faraday rotation is restricted to rather low frequencies, less than 10 THz, even at high magnetic fields (see white dashed lines in lower panels in Figure 2). As seen from Figure 3, graphene ribbon arrays, despite being a diluted one-atom thick material, still present values of θ_F of the order of a few degrees. Moreover, the frequency at which maximum θ_F occurs in ribbon arrays is strongly blue-shifted with respect to the one in a continuous graphene sheet. This difference is especially significant for low magnetic fields (less than a few Tesla). In the ribbon array, the maximum of Faraday rotation occurs at the resonance excitation of GMPs, which is determined by both ribbon width and magnetic field. At high magnetic fields, for which the fundamental GMP mode approaches the cyclotron resonance, the ribbon arrays have no obvious advantage over continuous graphene, even producing a weaker Faraday effect.

Figure 3c,d shows the corresponding transmittance spectra. Notice that minimum transmittance occurs approximately at the spectral position where θ_F changes sign. Importantly, the transmittance at maximum θ_F is ~85−90%, which allows increasing of the Faraday rotation by stacking vertically several layers of ribbon arrays, yet maintaining an appreciable transmitted field.

Associated to the Faraday rotation in graphene ribbons, there is a change in the polarization of the transmitted light. This is illustrated in Figure 4, which renders the ellipticity spectra of transmitted radiation for the two considered graphene ribbons, and for continuous graphene.

When the lattice parameter is much smaller than the free-space wavelength, we can use a metamaterial

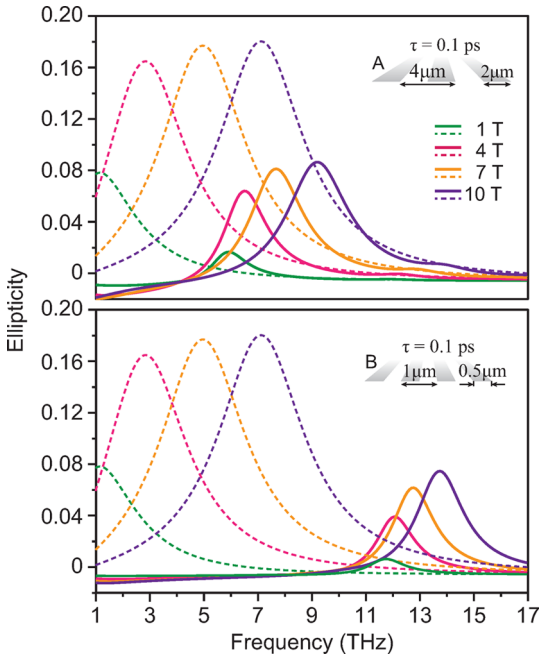

Figure 4. Frequency dependence of the ratio between the minor and major semiaxis of the polarization of transmitted radiation through both continuous graphene (dashed lines) and arrays of graphene ribbons (continuous lines). The considered geometrical parameters and scattering time are as in Figure 3.

approach and, for the computation of the scattering coefficients, represent the graphene ribbon array as a continuous monolayer with an effective conductivity tensor $\tilde{\sigma}(B)$. The two independent components of the effective conductivity tensor, namely, $\tilde{\sigma}_{xx}$ and $\tilde{\sigma}_{xy}$, can be uniquely derived from the zero-order transmission coefficients t_{0xx} and t_{0xy}. In particular, for the free-standing ribbons array, we obtain (see Supporting Information for the derivation):

$$\tilde{\sigma}_{xx} = \frac{c}{4\pi}\left[\frac{t_{0xx}}{t_{0xx}^2 + t_{0xy}^2} - 1\right]$$
$$\tilde{\sigma}_{xy} = \frac{c}{4\pi}\frac{t_{0xy}}{t_{0xx}^2 + t_{0xy}^2} \quad (4)$$

The lower panels of Figure 3 show the frequency dependence of both $Re\tilde{\sigma}_{xy}$ (for the two considered arrays) and $Re\sigma_{xy}$ (continuous graphene). Notice that the relation between the Faraday angle and nondiagonal component of the conductivity tensor, valid for low relaxation times, $\theta_F \simeq 4\pi c^{-1} \mathrm{Re}\sigma_{xy}$ can be still applied in the case of ribbon arrays (in which case $\theta_F \simeq 4\pi c^{-1} Re\tilde{\sigma}_{xy}$), as can be seen by comparing Figure 3e,f with 3a,b.

To better illustrate the magneto-optical response of the ribbon arrays, we define the effective magnetic field, B_{eff}, such that the spectral position of the maximum Faraday angle is the same for a *continuous* graphene sheet under the presence of B_{eff} and for the ribbon array under the actual B (with all other parameters like chemical potential μ_c, mobility, *etc.*, remaining the same). Figure 5a renders the dependence of the computed B_{eff} with B, for different arrays of ribbons, showing clearly that submicrometer graphene ribbons produce maxima in the Faraday rotation at frequencies that would only be achievable in a continuous graphene sheet at much larger magnetic fields. If these large magnetic field are achievable, a continuous sheet would produce a larger Faraday angle. This is illustrated in Figure 5c, which shows the ratio between $\theta_F(B_{eff})$ in a graphene sheet and $\theta_F(B)$ in the ribbon, $R(B) = \theta_F^{ribbon}(B)/\theta_F^{sheet}(B_{eff})$, evaluated at the resonant frequency. This figure shows that, for low relaxation times, the decrease in magnetic field needed to obtain high Faraday angles in ribbons, with respect to the situation in a continuous sheet, is accompanied by a decrease in the maximum Faraday angle ($R < 1$). As the magnetic field increases, so does R, and when the magnetic field is high enough (so that the magnetoplasmon frequency in ribbons tends to the cyclotron frequency) $R(B)$ is limited by the filling fraction w/L.

Another way to obtain Faraday rotation at higher frequencies in a continuous graphene sheet is by reducing the chemical potential μ_c. To compare the response of 2D graphene and the ribbon array, we define an effective chemical potential $\mu_c^{eff}(B)$ such that the spectral position of maximum θ_F is the same for a *continuous* graphene sheet at $\mu_c^{eff}(B)$ and for the ribbon array under the actual μ_c (with all other parameters like B, mobility, *etc.*, remaining the same). Figure 5b renders the $\mu_c^{eff}(B)$ for several ribbons arrays, for $\mu_c = 0.2$ eV. Notice, however, that the strategy of increasing the frequency of resonant Faraday rotation in a continuous sheet by decreasing the chemical potential is limited by the condition $\hbar\omega_c < 2\,\mu_c^{eff}$. In Figure 5c, this is reflected in the fact that the different curves have end-points at the lower chemical potentials that fulfill the previous condition. Notice also that, as shown in Figure 5d, ribbon arrays can provide, at a given magnetic field and a given frequency, a substantially larger Faraday rotation than a continuous graphene sheet. This occurs at magnetic fields such that $\mu_c^{eff} \ll \mu_c$, *i.e.*, when the resonance is magnetoplasmonic, rather than cyclotronic, in character.

Up to now we have considered a value for the carrier mobility in graphene that is routinely produced nowadays. However, in view of the recent advances in producing high-quality graphene samples, it is valuable to know whether there are physical limits to what can be achievable. A well-known example of these limits is that the maximum possible absorption by a free-standing infinitely thin sheet is 50%.[45] Concerning the change in polarization, we find that in a free-standing infinitely thin sheet, characterized by a local conductivity, the modulus of each of the zero-order cross-polarization amplitudes has a maximum value of 1/2 (see Supporting Information). This is,

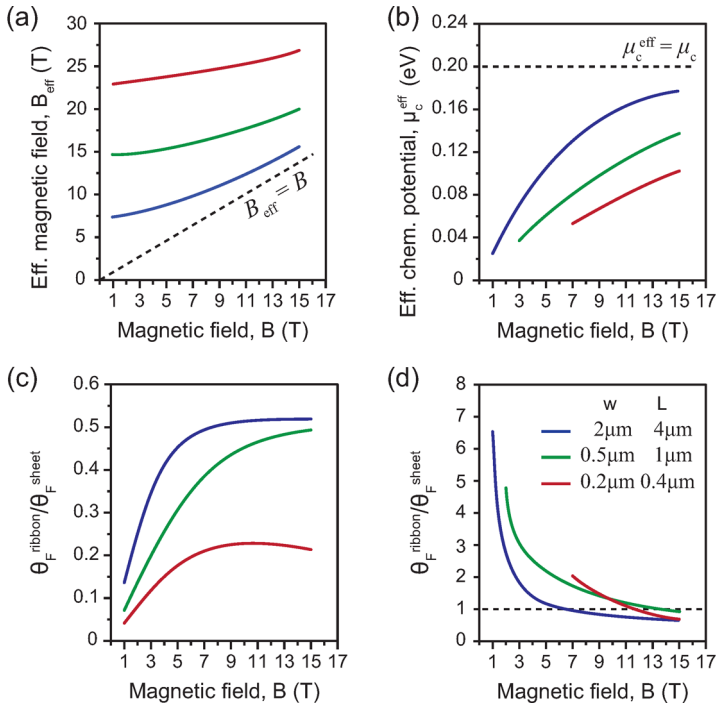

Figure 5. Effective magnetic field (a) and effective chemical potential (b), defined as those at which a continuous graphene sheet would produce maximum giant Faraday rotation at the same frequency as the ribbon array at a given magnetic field *B* (with all other parameters unchanged). The bottom panels render the ratio between the maximal Faraday angle of graphene ribbon arrays and that of the continuous sheet at the corresponding effective parameters (panel c for B_{eff} and panel d for μ_c^{eff}).

$$|t^{sp}|^2_{max} = |t^{ps}|^2_{max} = |r^{sp}|^2_{max} = |r^{ps}|^2_{max} = \frac{1}{4} \quad (5)$$

By structuring graphene, we cannot increase this limiting value. However, we can largely improve the resonance q-factor (the GMP resonance is less absorptive, see Figure 2a,b). This has implications for the Faraday rotation. In a continuous translational-invariant sheet, it can be shown (see Supporting Information) that, at not very low magnetic field and frequencies, the maximal Faraday angle is $|\theta_F|_{max} \simeq \pi/4$ which, of course, is already an impressive result, even more so for a one-atom-thick layer. Remarkably, Faraday rotation on graphene ribbon arrays can exceed this value. As was previously shown,[11] the transmission coefficient t_{0xx} can be very low. If we set $t_{0xx} \to 0$ in eq 2, we immediately obtain $|\theta_F| \to \pi/2$. These properties are illustrated in Figure 6, which shows the computed transmittance and Faraday angle, for both arrays A and B, for the case $\tau = 4.4$ ps. This figure shows that the Faraday angle strongly depends on scattering time and that in ribbons it may even exceed that of a continuous graphene sheet (and, as stated above, present maximum θ_F at larger frequencies).

In all the previous calculations, we have considered free-standing graphene ($\varepsilon_1 = \varepsilon_2 = 1$) because the fundamental physics we were discussing (the influence of excitation of GSP on the Faraday rotation) was already present in this simple configuration. Nevertheless, in practice, graphene is usually produced on a substrate. One consequence of this is that carrier

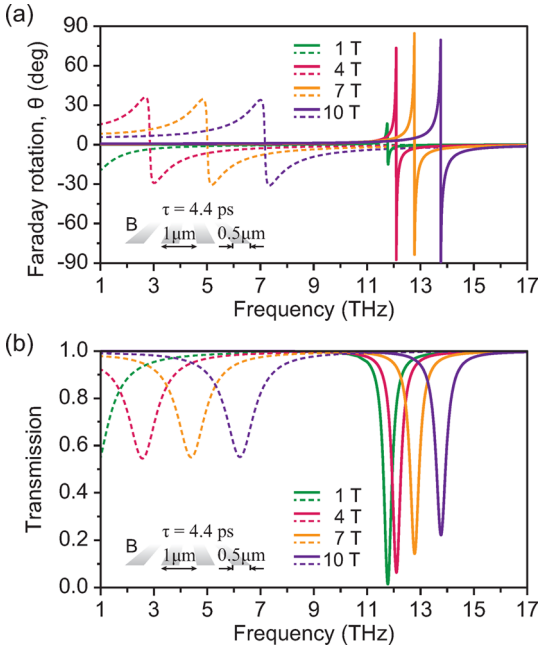

Figure 6. The results for ribbon arrays (solid curves) and continuous graphene (dashed curves) for the ultrahigh relaxation time $\tau = 4.4$ ps: (a) Faraday rotation at various magnetic fields; (b) zeroth-order transmission.

mobility is reduced, due to scattering with phonons and charged impurities. Additionally, although the presence of a substrate does not significantly affect the polarization rotation in a continuous graphene sheet, this may not be the case for graphene ribbons,

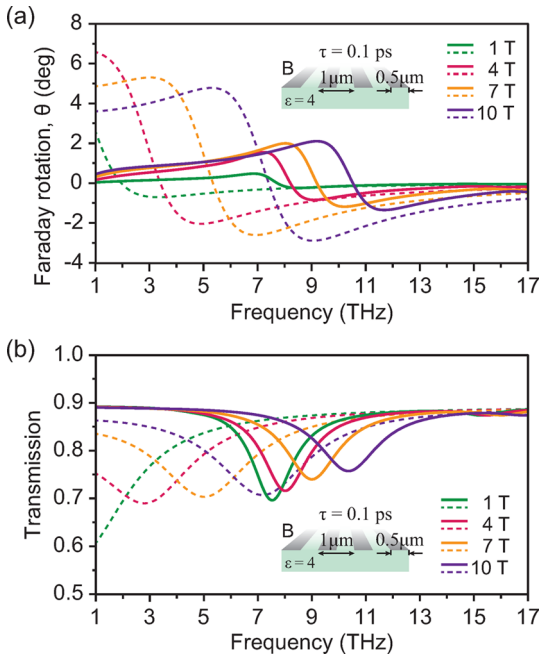

Figure 7. The results for ribbon arrays (solid curves) and continuous graphene (dashed curves) placed on top of the substrate with $\varepsilon = 4$: (a) Faraday rotation at various magnetic fields; (b) zeroth-order transmission. The relaxation time is $\tau = 0.1$ ps.

since plasmon excitations are very sensitive to the surrounding medium. The influence of a substrate on the GSP-enhanced Faraday rotation of graphene ribbons is exemplary illustrated in Figure 7, for one of the ribbon arrays considered in this work placed on a semi infinite substrate characterized by a nondispersive dielectric permittivity $\varepsilon_2 = 4$. As the figure shows, the blue shifts of the maximum in the Faraday angle occurring when graphene is patterned are still present, although they are reduced by the presence of the dielectric substrate (as can be seen by the comparison with Figure 3b).

CONCLUSION

We have shown that, for a given magnetic field and chemical potential, structuring graphene periodically can provide large Faraday rotation (more than 1°) at larger frequencies than what would occur in a continuous graphene sheet. Alternatively, at a given frequency, graphene ribbons produce large Faraday rotation at much smaller magnetic fields than those in continuous graphene. This is produced by the resonant coupling of radiation to the ribbon magnetoplasmons. The possibility to control the graphene magnetoplasmon frequency through both geometry and magnetic field, combined with the possibility to modify the carrier density by an external gate voltage, holds an exciting promise for designing dynamically tunable devices employing *solely* the magneto-optical properties of graphene.

METHODS

In this paper, we have used a standard Fourier-Floquet plane wave expansion method. We represent the fields in the upper and lower dielectric half-spaces in the form of an infinite sum of plane waves. The fields are then matched at the interface through the boundary conditions, which present the continuity of the parallel components of the electric fields and discontinuity of the parallel components of the magnetic fields due to the presence of the graphene monolayer. The resulting infinite system of equations for the amplitudes of the plane waves is truncated and solved numerically; the truncation is controlled by the convergency of the solution. All the calculations have also been verified by finite elements methods using Comsol software.

Conflict of Interest: The authors declare no competing financial interest.

Acknowledgment. This work has been partially funded by the Spanish Ministry of Science and Innovation under Contract MAT2011-28581-C02.

Supporting Information Available: Additional figures and computational details. This material is available free of charge *via* the Internet at http://pubs.acs.org.

REFERENCES AND NOTES

1. Shamir, J. *Optical Systems and Processes*; SPIE: Bellingham, WA, 2006.
2. Hopster, H.; Oepen, H. P. *Magnetic Microscopy of Nanostructures*; Springer: Berlin; New York, 2005.
3. Sepulveda, B.; Gonzalez-Diaz, J. B.; Garcia-Martin, A.; Lechuga, L. M.; Armelles, G. Plasmon-Induced Magneto-Optical Activity in Nanosized Gold Disks. *Phys. Rev. Lett.* **2010**, *104*, 147401.
4. Sounas, D. L.; Caloz, C. Electromagnetic Nonreciprocity and Gyrotropy of Graphene. *Appl. Phys. Lett.* **2011**, *98*, 021911.
5. Crassee, I.; Levallois, J.; Walter, A. L.; Ostler, M.; Bostwick, A.; Rotenberg, E.; Seyller, T.; van der Marel, D.; Kuzmenko, A. B. Giant Faraday Rotation in Single- and Multilayer Graphene. *Nat. Phys.* **2010**, *7*, 48–51.
6. Fallahi, A.; Perruisseau-Carrier, J. Manipulation of Giant Faraday Rotation in Graphene Metasurfaces. *Appl. Phys. Lett.* **2012**, *101*, 231605.
7. Crassee, I.; Orlita, M.; Potemski, M.; Walter, A. L.; Ostler, M.; Seyller, T.; Gaponenko, I.; Chen, J.; Kuzmenko, A. B. Intrinsic Terahertz Plasmons and Magnetoplasmons in Large Scale Monolayer Graphene. *Nano Lett.* **2012**, *12*, 2470–2474.
8. Ju, L.; Geng, B.; Horng, J.; Girit, C.; Martin, M.; Hao, Z.; Bechtel, H. A.; Liang, X.; Zettl, A.; Shen, Y. R.; *et al.* Graphene Plasmonics for Tunable Terahertz Metamaterials. *Nat. Nanotechnol.* **2011**, *6*, 630–634.
9. Koppens, F. H. L.; Chang, D. E.; Garcia de Abajo, F. J. Graphene Plasmonics: A Platform for Strong Light-Matter Interactions. *Nano Lett.* **2011**, *11*, 3370–3377.
10. Nikitin, A. Y.; Guinea, F.; Garcia-Vidal, F. J.; Martin-Moreno, L. Edge and Waveguide Terahertz Surface Plasmon Modes in Graphene Microribbons. *J. Appl. Phys.* **2011**, *84*, 161407.
11. Nikitin, A. Y.; Guinea, F.; Garcia-Vidal, F. J.; Martin-Moreno, L. Surface Plasmon Enhanced Absorption and Suppressed Transmission in Periodic Arrays of Graphene Ribbons. *Phys. Rev. B* **2012**, *85*, 081405(R).
12. Fang, Z.; Wang, Y.; Liu, Z.; Schlather, A.; Ajayan, P. M.; Koppens, F. H. L.; Nordlander, P.; Halas, N. J. Plasmon-Induced Doping of Graphene. *ACS Nano* **2012**, *6*, 10222–10228.
13. Gao, W.; Shu, J.; Qiu, C.; Xu, Q. Excitation of Plasmonic Waves in Graphene by Guided-Mode Resonances. *ACS Nano* **2012**, *6*, 7806–7813.
14. Vasić, B.; Isić, G.; Gajić, R. Localized Surface Plasmon Resonances in Graphene Ribbon Arrays for Sensing of

Dielectric Environment at Infrared Frequencies. *J. Appl. Phys.* **2013**, *113*, 013110.
15. Fang, Z.; Thongrattanasiri, S.; Schlather, A.; Liu, Z.; Ma, L.; Wang, Y.; Ajayan, P. M.; Nordlander, P.; Halas, N. J.; Garcia de Abajo, F. J. Gated Tunability and Hybridization of Localized Plasmons in Nanostructured Graphene. *ACS Nano* **2013**, *7*, 2388–2395.
16. Chiu, K. W.; Quinn, J. J. Plasma Oscillations of a Two-Dimensional Electron Gas in a Strong Magnetic Field. *Phys. Rev. B* **1974**, *9*, 4724–4732.
17. Kukushkin, I. V.; Muravev, V. M.; Smet, J. H.; Hauser, M.; Dietsche, W.; von Klitzing, K. Collective Excitations in Two-Dimensional Electron Stripes: Transport and Optical Detection of Resonant Microwave Absorption. *Phys. Rev. B* **2006**, *73*, 113310.
18. Bychkov, Y. A.; Martinez, G. Magnetoplasmon Excitations in Graphene for Filling Factors $\nu \ll 6$. *Phys. Rev. B* **2008**, *77*, 125417.
19. Berman, O. L.; Gumbs, G.; Lozovik, Y. E. Magnetoplasmons in Layered Graphene Structures. *Phys. Rev. B* **2008**, *78*, 085401.
20. Ferreira, A.; Peres, N. M. R.; Castro Neto, A. H. Confined Magneto-Optical Waves in Graphene. *Phys. Rev. B* **2012**, *85*, 205426.
21. Sounas, D. L.; Caloz, C. Edge Surface Modes in Magnetically Biased Chemically Doped Graphene Strips. *Appl. Phys. Lett.* **2011**, *99*, 231902.
22. Fischer, A. M.; Römer, R. A.; Dzyubenko, A. B. Magnetoplasmons and SU(4) Symmetry in Graphene. *J. Phys.: Conf. Ser.* **2011**, *286*, 012054.
23. Balev, O. G.; Vasilopoulos, P.; Frota, H. O. Edge Magnetoplasmons in Wide Armchair Graphene Ribbons. *Phys. Rev. B* **2011**, *84*, 245406.
24. Gómez-Díaz, J. S.; Perruisseau-Carrier, J. Propagation of Hybrid Transverse Magnetic-Transverse Electric Plasmons on Magnetically Biased Graphene Sheets. *J. Appl. Phys.* **2012**, *112*, 124906.
25. Chin, J. Y.; Steinle, T.; Wehlus, T.; Dregely, D.; Weiss, T.; Belotelov, V. I.; Stritzker, B.; Giessen, H. Nonreciprocal Plasmonics Enables Giant Enhancement of Thin-Film Faraday Rotation. *Nat. Commun.* **2013**, *4*, 1599.
26. Bludov, V.; Yu, M. I.; Vasilevskiy, M. I.; Peres, N. M. R. Tunable Graphene-Based Polarizer. *J. Appl. Phys.* **2012**, *112*, 084320.
27. Ferreira, A.; Viana-Gomes, J.; Bludov, Y. V.; Pereira, V.; Peres, N. M. R.; Castro Neto, A. H. Faraday Effect in Graphene Enclosed in an Optical Cavity and the Equation of Motion Method for the Study of Magneto-Optical Transport in Solids. *Phys. Rev. B* **2011**, *84*, 235410.
28. Gusynin, V. P.; Sharapov, S. G.; Carbotte, J. P. On the Universal AC Optical Background in Graphene. *New J. Phys.* **2009**, *11*, 095013.
29. Orlita, M.; Faugeras, C.; Plochocka, P.; Neugebauer, P.; Martinez, G.; Maude, D. K.; Barra, A.-L.; Sprinkle, M.; Berger, C.; de Heer, W. A.; *et al.* Approaching the Dirac Point in High-Mobility Multilayer Epitaxial Graphene. *Phys. Rev. Lett.* **2008**, *101*, 267601.
30. Morozov, S. V.; Novoselov, K. S.; Katsnelson, M. I.; Schedin, F.; Elias, D. C.; Jaszczak, J. A.; Geim, A. K. Giant Intrinsic Carrier Mobilities in Graphene and Its Bilayer. *Phys. Rev. Lett.* **2008**, *100*, 016602.
31. Hwang, E.; Das Sarma, S. Acoustic Phonon Scattering Limited Carrier Mobility in Two-Dimensional Extrinsic Graphene. *Phys. Rev. B* **2008**, *77*, 115449.
32. Chen, J.-H.; Jang, C.; Xiao, S.; Ishigami, M.; Fuhrer, M. S. Intrinsic and Extrinsic Performance Limits of Graphene Devices on SiO_2. *Nat. Nanotechnol.* **2008**, *3*, 206–209.
33. We have used the implementation of the finite element method provided by the commercial software COMSOL Multiphysics.
34. Fialkovsky, I.; Vassilevich, D. V. Parity-Odd Effects and Polarization Rotation in Graphene. *J. Phys. A: Math. Theor.* **2009**, *42*, 442001.
35. Alaee, R.; Farhat, M.; Rockstuhl, C.; Lederer, F. A perfect Absorber Made of a Graphene Micro-Ribbon Metamaterial. *Opt. Express* **2012**, *20*, 28017.
36. Yan, H.; Low, T.; Zhu, W.; Wu, Y.; Freitag, M.; Li, X.; Guinea, F.; Avouris, P.; Xia, F. Damping Pathways of Mid-Infrared Plasmons in Graphene Nanostructures. *Nat. Photonics* **2013**, *7*, 394–399.
37. Eliasson, G.; Wu, J.-W.; Hawrylak, P.; Quinn, J. J. Magnetoplasma Modes of a Spatially Periodic Two-Dimensional Electron Gas. *Solid State Commun.* **1986**, *60*, 41–44.
38. Mikhailov, S.; Savostianova, M. Microwave Response of a Two-Dimensional Electron Stripe. *Phys. Rev. B* **2005**, *71*, 035320.
39. Demel, T.; Heitmann, D.; Grambow, P.; Ploog, K. Far-Infrared Response of One-Dimensional Electronic Systems in Single- and Two-Layered Quantum Wires. *Phys. Rev. B* **1988**, *38*, 12732–12735.
40. Demel, T.; Heitmann, D.; Grambow, P.; Ploog, K. One-Dimensional Plasmons in AlGaAs/GaAs Quantum Wires. *Phys. Rev. Lett.* **1991**, *66*, 2657–2660.
41. Zhao, H. L.; Zhu, Y.; Wang, L.; Feng, S. Magnetoplasmons in a Quasi-One-Dimensional Quantum Wire. *J. Phys.: Condens. Matter* **1994**, *6*, 1685.
42. Kukushkin, I. V.; Smet, J. H.; Kovalskii, V. A.; Gubarev, S. I.; von Klitzing, K.; Wegscheider, W. Spectrum of One-Dimensional Plasmons in a Single Stripe of Two-Dimensional Electrons. *Phys. Rev. B* **2005**, *72*, 161317.
43. Mikhailov, S. A.; Savostianova, N. A. Microwave Response of a Two-Dimensional Electron Stripe: Electrodynamics and The Influence of Contacts. *Int. J. Mod. Phys. B* **2007**, *21*, 1497–1501.
44. Fedorych, O. M.; Studenikin, S. A.; Moreau, S.; Potemski, M.; Saku, T.; Hirayama, Y. Microwave Magnetoplasmon Absorption by a 2DEG Stripe. *Int. J. Mod. Phys. B* **2009**, *23*, 2698.
45. Thongrattanasiri, S.; Koppens, F. H. L.; García de Abajo, F. J. Complete Optical Absorption in Periodically Patterned Graphene. *Phys. Rev. Lett.* **2012**, *108*, 047401.